SCIENCE CHINA
Information Sciences

• RESEARCH PAPER •

December 2023, Vol. 66 222403:1–222403:8
https://doi.org/10.1007/s11432-023-3841-9

Proximity-induced magnetic order in topological insulator on ferromagnetic semiconductor

Hangtian WANG[1,2†], Koichi MURATA[3†], Weiran XIE[1†], Jing LI[1], Jie ZHANG[1*], Kang L. WANG[3], Weisheng ZHAO[1,2] & Tianxiao NIE[1,2*]

[1]*School of Integrated Circuit Science and Engineering and Advanced Innovation Center for Big Data and Brain Computing, Beihang University, Beijing* 100191*, China;*
[2]*Beihang-Goertek Joint Microelectronics Institute, Qingdao Research Institute, Beihang University, Qingdao* 266000*, China;*
[3]*Department of Electrical Engineering, University of California, Los Angeles* 90095*, USA*

Received 11 March 2023/Revised 3 June 2023/Accepted 4 August 2023/Published online 8 November 2023

Abstract Introducing magnetic order into topological insulator (TI) to break the time-reversal symmetry can yield numerous fascinating physical phenomena, which brings new hope for the emerging spintronic technology. The proximity effect is regarded as a promising strategy that could advance the step for realistic application by choosing a suitable ferromagnetic layer with the merits of high Curie temperature and high compatibility with mainstream semiconductor technology. Here, we prepare a Bi_2Se_3 thin film on Si-compatible ferromagnetic semiconductor (FMS) of Mn_xGe_{1-x} by molecular beam epitaxy. After integration, the nonmagnetic Bi_2Se_3 exhibits an anomalous Hall signal and a clear weak localization cusp in magnetoresistance until 150 K, confirming that a high-temperature magnetism can be induced by the proximity effect. Detailed investigation of the magnetoconductance quantitatively indicates that the Bi_2Se_3 conductance suffers a transition from weak antilocalization to weak localization behavior after integrating with Mn_xGe_{1-x}, and an 80 meV bandgap is predicted to be opened in the surface states in Bi_2Se_3 layer due to the proximity-induced magnetism. Our results prove that the proximity effect could be an important method to achieve topological magnetism at high temperatures, and reveals its potential for the manipulation of the topological surface states.

Keywords topological insulator, ferromagnetic semiconductor, proximity effect, quantum interference

Citation Wang H T, Murata K, Xie W R, et al. Proximity-induced magnetic order in topological insulator on ferromagnetic semiconductor. Sci China Inf Sci, 2023, 66(12): 222403, https://doi.org/10.1007/s11432-023-3841-9

1 Introduction

With the development of integrated circuit technology, spintronic devices have become a research hotspot [1–4]. The nontrivial band topology and strong spin-orbit coupling endow the topological insulator (TI) with a time-reversal symmetry (TRS) protected topological surface state, which significantly inspired numerous research in developing TI-based low-power consumption spintronic devices. Magnetic topological insulator (MTI) is considered one of the core interests in this field. With additional ferromagnetic orders introduced in TI, the breaking of surface TRS gives rise to abundant exotic properties, such as topological magnetoelectric effect [5], magnetic monopole [6], and quantum anomalous Hall effects [7–9]. Traditionally, a long-range ferromagnetic order could be generated by doping transition metals such as Cr [10, 11], V [12], and Mn [13, 14] in TI, which was attributed to two major mechanisms called Ruderman-Kittel-Kasuya-Yosida (RKKY) interaction and van Vleck mechanism [10]. However, the magnetic phase induced by doping may not distribute in TI uniformly due to the random distribution of the magnetic impurities, which will also cause inevitable damage to the crystal structure of TI. Moreover, previous experiments have proven that incorporating dopants can only sustain the ferromagnetic order at extremely low temperatures (<45 K) [15], which is much lower than the demand for practical application.

* Corresponding author (email: zhangjie2019@buaa.edu.cn, nietianxiao@buaa.edu.cn)
† Wang H T, Murata K, and Xie W R have the same contribution to this work.

© Science China Press 2023

Alternatively, the magnetic proximity effect provides an effective way to achieve the ferromagnetism order in TI at high temperatures. Through interfacial exchange coupling, the adjacent ferromagnet could give rise to ferromagnetism in the TI surface without disturbing the original crystal structure. Recent progress in TI-based heterostructures has proven such feasibility. However, neither ferromagnetic insulators (such as EuS [16] and $CrGeTe_3$ [17]), ferrimagnetic insulators (YIG [18], TIG [19]) nor antiferromagnets (CrSb [20], MnTe [21]) could be well compatible with modern semiconductor technology, which may impair the incorporation of TI with mainstream IC devices. Therefore, hiring new magnetic candidates with controllable magnetic anisotropy, easy-tuning conductivity, and high compatibility with mature semiconductor technology is important for the development and implementation of TI in spintronics.

Ferromagnetic semiconductor (FMS) appears to be a promising candidate to satisfy such demand, which can be fabricated by magnetic doping in semiconductor materials. FMS could be well controlled in its conductance and ferromagnetism by tuning the doping level and manifests an electric-field control of ferromagnetism through RKKY interaction [22, 23]. Among various FMSs, Mn_xGe_{1-x} usually demonstrates high compatibility with the semiconductor technology and possesses a high Curie temperature (T_c) [24, 25]. More importantly, Mn_xGe_{1-x} has a relatively small lattice mismatch with commonly-used TI, such as Bi_2Se_3 and Bi_2Te_3 [26]. All these extraordinary properties make Mn_xGe_{1-x} one of the most promising candidates to enhance the proximity effect in TI with stable ferromagnetism and high working temperature. However, there is no report yet on the proximity effect from high-quality TI/Mn_xGe_{1-x} heterostructure.

In this work, Bi_2Se_3/Mn_xGe_{1-x} ($x = 0.04$) heterostructure was successfully grown by molecular beam epitaxy (MBE). By precisely controlling the doping concentration, the conductance of Mn_xGe_{1-x} was tuned to minimize to avoid the potential shunting effect on Bi_2Se_3. Through the transport measurement, the typical negative cusp in the magnetoresistance curve verifies that magnetism was induced in Bi_2Se_3 by the interfacial proximity effect with its T_c over 150 K. Subsequently, we revealed a magnetism-induced bandgap opening in the surface states of the Bi_2Se_3 layer by quantifying the transition from weak antilocalization (WAL) to weak localization (WL) feature. Compared with pure TI which was dominated by WAL, the transport property of the heterostructure contains both WAL and WL signals, indicating the TRS broken by magnetism in the Bi_2Se_3 layer. To determine the contribution of the proximity-induced magnetism on the surface states, a further calculation was performed by extracting the WAL and WL prefactor in the quantum interferences, and we predicted that an 80 meV surface bandgap could be opened in the Bi_2Se_3 layer, demonstrating a stable ferromagnetic order introduced by the proximity effect in the heterostructure.

2 Results and discussions

A 20 nm-thick Mn_xGe_{1-x} thin film was grown on a commercial GaAs (111) B substrate in our MBE system. Inheriting the structure of Ge crystal, Mn_xGe_{1-x} has a cubic crystal structure with a lattice constant of 5.65 Å. Here the Mn doping concentration of Mn_xGe_{1-x} is around 4% and each Mn atom randomly occupies the position of Ge in the unit cell, as shown in Figure 1(a). Then 8 nm Bi_2Se_3 was deposited on the Mn_xGe_{1-x} to fabricate a heterostructure. Here, the substrate temperature was strictly controlled at 200°C. Otherwise, a Ge-Se impurity phase will be formed (Figure A1 in the Supplementary File). X-ray diffraction (XRD) was employed to characterize the crystal structure of the heterostructure and a typical result is shown in Figure 1(b). Mn_xGe_{1-x} {111} peak exhibits the strongest intensity and other diffraction peaks correspond to Bi_2Se_3 {003} family planes (according to the PDF card of #15-0863 [27]), indicating that no other impurity phase was formed. During the growth, the reflection high-energy electron diffraction (RHEED) was used to monitor the deposition, and the pattern of the heterostructure is shown in the inset of Figure 1(b). For the initial growth, a sharp streaky RHEED pattern of Mn_xGe_{1-x} thin film could be observed, indicating a smooth surface morphology. The lattice mismatch of Mn_xGe_{1-x} and Bi_2Se_3 is 3.6%, which is relatively smaller than other substrates for Bi_2Se_3, and the van der Waals growth of topological insulators helps the heterostructure to overcome the mismatch, promising the perfect quality of the interface. After growth, a streaky pattern can also be observed from the Bi_2Se_3 film, demonstrating a 2D surface of the Bi_2Se_3 film. The perfect surface morphology was further confirmed by atomic force microscopy (AFM), as shown in Figure 1(c), which shows a typical terrace structure similar to already reported TI results [27]. The quality of the interface was investigated by high-resolution

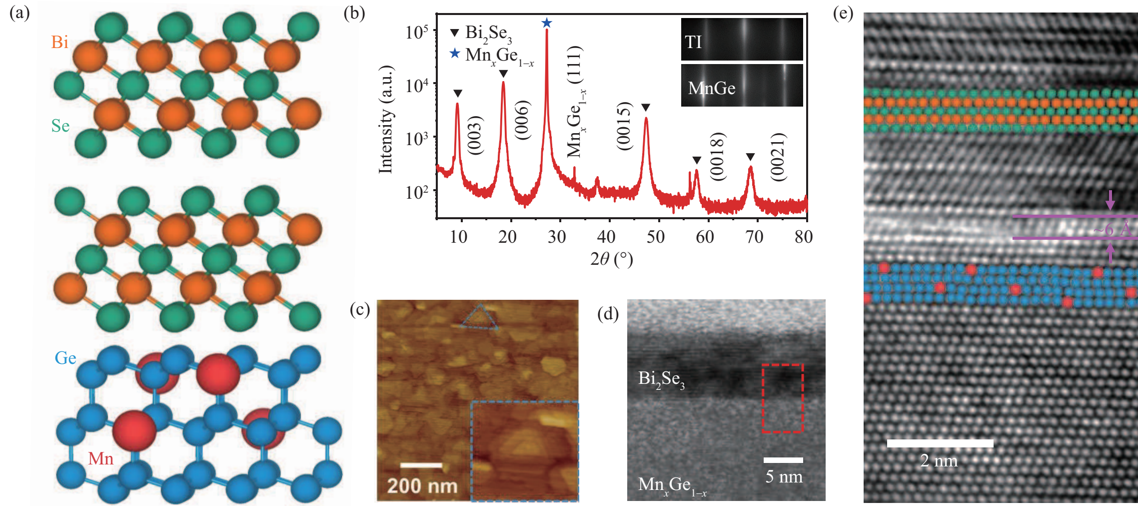

Figure 1 (Color online) Characterization of the Bi_2Se_3/Mn_xGe_{1-x} ($x = 0.04$) heterostructure. (a) The schematic diagram of the lattice structure of the heterostructure. Mn_xGe_{1-x} inherits the crystal structure of Ge with 4% Mn atoms distributing in the unit randomly. (b) XRD spectrum of the heterostructure. Except for Mn_xGe_{1-x} {111}, only peaks belonging to Bi_2Se_3 {003} family can be observed. Inset: RHEED patterns along ⟨11-20⟩ direction of the sample, which show a sharp 2D pattern for Mn_xGe_{1-x} and Bi_2Se_3. (c) AFM image of the heterostructure with the area of 1 μm × 1 μm. Inset: a typical terrace feature belonging to Bi_2Se_3 crystal. (d) and (e) TEM images of the sample. The heterostructure has a well-epitaxial crystal structure for both Bi_2Se_3 and Mn_xGe_{1-x} layers.

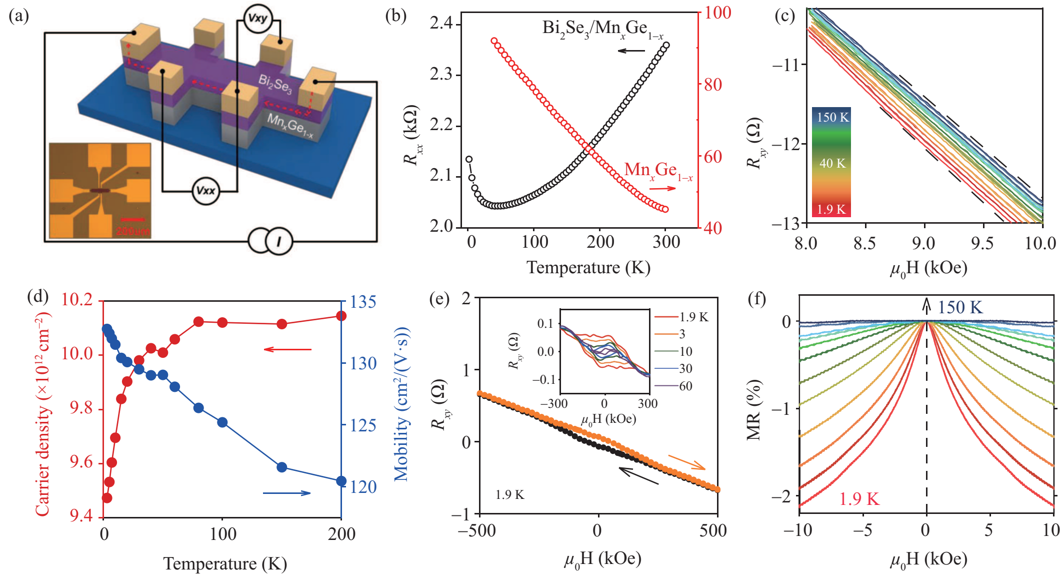

Figure 2 (Color online) The transport measurement for Bi_2Se_3/Mn_xGe_{1-x} ($x = 0.04$) heterostructure. (a) A schematic diagram of the Hall-bar device. The inset shows the optical micrograph of the device. (b) The R_{xx}-T curves for pure Mn_xGe_{1-x} and Bi_2Se_3/Mn_xGe_{1-x}. The resistance of the heterostructure is much larger than pure Mn_xGe_{1-x} at all temperatures. (c) Zoom-in Hall curves for the heterostructure. (d) The exacted 2D carrier concentrations and mobility of the heterostructure. (e) The Hall curve of the heterostructure at 1.9 K. The inverse AHE response indicates the opposite magnetic direction between the upper Mn_xGe_{1-x} and lower Bi_2Se_3 layer. Inset: The anomalous Hall resistance extracted from Hall curves, which degrades as the temperature increases. (f) The magnetoresistance curves of the heterostructure, which show a negative cusp belonging to the WL feature until 150 K.

transmission electron microscopy (HRTEM), as shown in Figures 1(d) and (e). The HRTEM result demonstrates a thin amorphized gap of 6 Å, above which the first Bi_2Se_3 layer develops. Except that, our heterostructure has a good crystal structure for Mn_xGe_{1-x} and Bi_2Se_3 layers.

To investigate the magnetic property of the heterostructure, the sample of $Bi_2Se_3(8)/Mn_xGe_{1-x}(20)$ ($x = 0.04$) was fabricated into a micrometer-sized Hall-bar device (shown in Figure 2(a)), and the physical property measurement system (PPMS) was employed to carry out the transport measurement. For clarity, an 8 nm-thick Bi_2Se_3 and 20 nm-thick Mn_xGe_{1-x} ($x = 0.04$) thin film on Ge (111) substrate was

measured as control groups. Owing to the deliberate manipulation of the stoichiometry during the sample preparation, the conductance of the Mn_xGe_{1-x} layer was tuned to minimize to promise the current flow mainly from the Bi_2Se_3 layer in the heterostructure, as shown by the red line in Figure 2(a). Figure 2(b) shows the temperature-dependent resistance (R-T curve) of the Bi_2Se_3/Mn_xGe_{1-x} heterostructure and Mn_xGe_{1-x}, respectively. The resistance of Mn_xGe_{1-x} is much larger than the heterostructure, proving that the transport property of the bilayer is dominated by Bi_2Se_3's conductance channel. Notably, the heterostructure resistance decreases as the temperature decreases from 300 to 50 K, manifesting a metallic behavior, which was also observed in pure TI [27,28]. When the temperature is below 50 K, the resistance increases as the temperature decreases because the bulk carriers in Bi_2Se_3 begin to freeze out and the surface channel dominates the conductance of the heterostructure. Figure 2(d) summarizes the carrier density and mobility of the heterostructure as a function of the temperature, which was extracted from the out-of-plane Hall signal in Figure 2(c). When the temperature reaches 200 K and the sheet electron density ($n_{\rm 2D}$) is around $10.2 \times 10^{12}\,{\rm cm}^{-2}$, the value is consistent well with previous reports majoring in pure Bi_2Se_3 [27, 28]. As the temperature decreases, the sheet carrier density continuously reduces with a sharp drop occurring at $\sim$60 K, which proves again that the low temperature will suppress the bulk conductance channel via carrier freezing.

Considering the leading role of Bi_2Se_3 in the heterostructure conductance, we extracted the anomalous Hall signal from Figure 2(c) to study the magnetic property of the Bi_2Se_3 layer, as shown in the inset of Figure 2(e). For the magnetic sample, the Hall resistivity (R_{xy}) could be divided into two parts: $R_{xy} = R_{\rm o} \cdot H + R_{\rm A} \cdot M$. Here, H is the magnetic field, M presents the magnetization, $R_{\rm o}$ and $R_{\rm A}$ are the coefficients of ordinary Hall and anomalous Hall effect (AHE), respectively. Within a small external field, the AHE component determines the Hall resistivity and manifests the magnetic property of the sample. For the heterostructure, the square anomalous Hall curves until 60 K indicate that magnetism is induced in the Bi_2Se_3 layer. Considering that no hysteresis loop was observed in pure Bi_2Se_3 (the inset of Figure A2(a)), the magnetism in the Bi_2Se_3 layer may come from the interfacial effect or the Mn segregation from the Mn_xGe_{1-x} layer. However, previous reports have never observed an AHE signal with clear coercivity in Mn-doped Bi_2Se_3 [29, 30]. Therefore, we conclude that the interfacial proximity is the reason for the magnetism in Bi_2Se_3 in this work. The negative AHE curve could also prove this conclusion (Figure 2(e)), in which the forward and reverse branch is shifted in opposite direction along the magnetic field as compared with normal hysteresis. Generally, a positive-sign AHE signal could be observed in magnetically doped Bi_2Se_3 [12, 31]. In this work, owing to the antiferromagnetic coupling between Bi_2Se_3 and Mn_xGe_{1-x}, the proximity-induced opposite magnetization will lead to a negative AHE signal. Figure 2(f) shows the temperature-dependent magnetoresistance (MR) curves of the heterostructure. With a negative MR cusp, the transport property of the heterostructure exhibits a typical WL feature until 150 K. However, for pure Bi_2Se_3, the MR curve should present a positive cusp because of the π-Berry phase in topological surface states. In the quantum diffusion regime, the quantum interferences in magnetic samples have a strong contribution to current, leading to an enhancement of the probability of electron backscattering as well as the resistance, which is the reason for WL and its contribution to conductance is called quantum correction [32]. However, for topological surface states with a π-Berry phase, this interference can be destroyed by the strong spin-orbital coupling, decreasing the probability of the occurrence of electron backscattering and resulting in an overall decrease of electrical resistance, which was called WAL effect WAL, but the WL can be recovered through breaking the π-Berry phase by introducing a magnetism [18, 33]. Thus, we conclude that such WL curves in Figure 2(f) come from the induced magnetism in the heterostructure, and the $T_{\rm c}$ of the magnetism is over 150 K. Notably, the value of magnetoresistance is one order larger than that from pure Mn_xGe_{1-x} film (Figure A2 in Appendix A), proving again the ferromagnetism is induced in the Bi_2Se_3 layer.

To quantitatively understand the relation between the proximity-induced ferromagnetism and the TRS-protected topological surface states, the magnetoconductivity (MC) $\Delta\sigma(B) = \sigma(B) - \sigma(0)$ of pure Bi_2Se_3 and the heterostructure were investigated, respectively. Due to the bulk freezing at low temperatures, the conductance of TI is dominated by surface states and should exhibit a WAL feature. Therefore, as shown in Figure 3(a), all MC curves in pure Bi_2Se_3 film display a typical negative cusp. Such behavior can be fitted via the single-component Hikami-Larkin-Nagaoka (HLN) formula [34]

$$\Delta\sigma(B) = \frac{\alpha e^2}{2\pi^2\hbar}\left[\Psi\left(\frac{l_B^2}{l_\Phi^2} + \frac{1}{2}\right) - \ln\left(\frac{l_B^2}{l_\Phi^2}\right)\right], \tag{1}$$

where Ψ is the digamma function, l_Φ is the phase coherence length, l_B is the magnetic length which

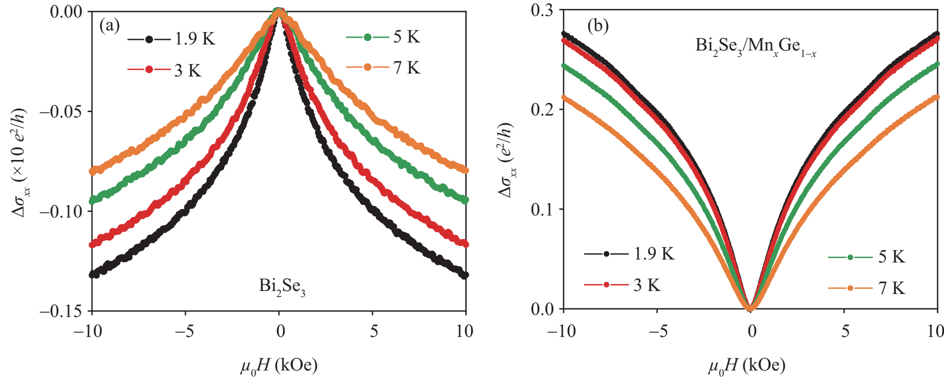

Figure 3 (Color online) The transition from WAL to WL in pure Bi_2Se_3 and $Bi_2Se_3/Mn_xGe_{1-x}(x = 0.04)$ heterostructure. (a) MC of the pure Bi_2Se_3 sample, which displays a typical WAL cusp. (b) MC of the heterostructure. The WAL component is suppressed and a positive WL cusp appears due to the magnetism induced by the proximity effect.

can be given by $l_B = (\hbar/4e|B|)^{1/2}$, and α is the WAL prefactor that quantifies its contribution to the quantum interference. For ideal TI with surface states, the maximum value of α is -0.5 because only one WAL channel dominates the conductance. In this work, fitting the MC data by the HLN formula yields an α near -0.4, as shown by the blue line in Figure 4(a). This value is slightly higher than the ideal value, which may be contributed to the defects in the surfaces of Bi_2Se_3 [35]. By contrast, after integrating with the Mn_xGe_{1-x} layer, the magnetism induced by the proximity effect in Bi_2Se_3 changes the negative cusp to positive due to the TRS breaking (Figure 3(b)), and the data cannot be simply captured by (1) because the exchange gap opened in the surface states leads to a WL component while suppressing the WAL effect [36]. To distinguish the contribution of these two effects, a two-component HLN formula is employed as [37]

$$\Delta\sigma(B) = \sum_{i=1,2} \frac{\alpha_i e^2}{2\pi^2\hbar} \left[\Psi\left(\frac{l_B^2}{l_{\Phi i}^2} + \frac{1}{2}\right) - \ln\left(\frac{l_B^2}{l_{\Phi i}^2}\right) \right], \tag{2}$$

where the magnetoconductivity consists of two ingredients: $i = 1$ and $i = 2$ represent the contribution of WAL and WL, respectively; α_i and $l_{\Phi i}$ are the corresponding prefactor and phase coherence length [38]. When the surface state is gapless, the system falls in the WAL regime with $\alpha_1 = -0.5$ and $\alpha_2 = 0$. If the surface state gap is opened by the magnetism, the quantum correction can be driven into the WL regime $\alpha_1 = 0$ and $\alpha_2 = 0.5$.

Following (2), the transition from WAL to WL for the pure Bi_2Se_3 and the heterostructure can be identified by extracting the prefactor α as well as the phase coherence length l_Φ from fitting the MC in Figures 3(a) and (b), and all the fitting parameters are plotted in Figures 4(a) and (b). Different from the pure Bi_2Se_3 in which the WAL prefactor α_1 keeps close to -0.5, α_1 for the heterostructure deceases to -0.2, indicating the suppressed WAL component, while the WL begins to dominate the conductance channel with a prefactor α_2 = 0.3–0.4. This transition from WAL to WL confirms the magnetism induced by the proximity as well as the TRS breaking in the surface states in the Bi_2Se_3 layer of the heterostructure. Despite the temperature changes, the α value for the heterostructure stays almost constant, demonstrating the strong proximity effect. In contrast, l_Φ varies with temperature, which can be described by a power law function as $T^{-\beta}$, where the ideal value of β is near 0.5 in 2D systems [39]. In this work, the extracted $l_\Phi^{\rm TI}$ and $l_\Phi^{\rm Bilayer}$ in the WAL component well match such power law function with a $\beta \sim 0.42$, demonstrating that the carrier transport is mostly 2D-like in the Bi_2Se_3 layer. The value of $l_\Phi^{\rm Bilayer}$ is slightly lower than $l_\Phi^{\rm TI}$, which is because the vanish of the Berry phase reduces the phase coherence length in quantum diffusive transport [33]. After integrating with Mn_xGe_{1-x}, the crossover from WAL to WL in the Bi_2Se_3 layer demonstrates the presence of the surface bandgap due to the magnetism induced by the proximity effect.

Here we calculate the quantum correction on the conductance induced by WAL and WL components in the heterostructure; then the calculated value is compared with the experimental values to verify the accuracy of our fitting results. Figure 4(c) shows the temperature-dependent conductivity for pure Bi_2Se_3 and Bi_2Se_3/Mn_xGe_{1-x} heterostructure; both curves present a logarithmical increase within the low-temperature region; the corresponding R_{xx}-T and σ_{xx}-T curves are plotted in Figure A3 in the

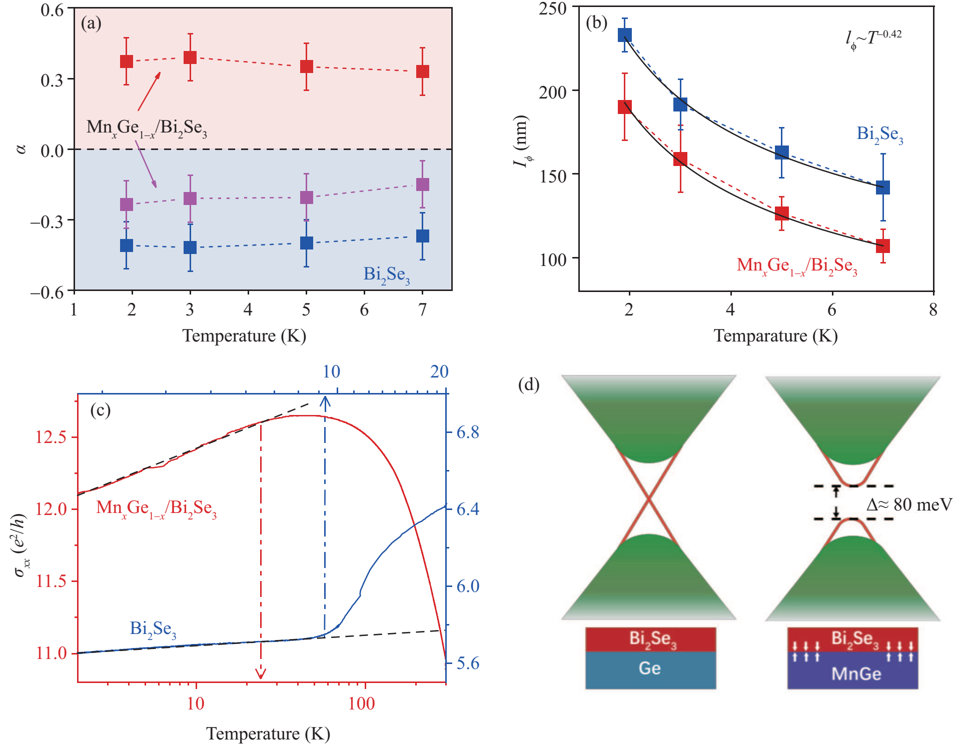

Figure 4 (Color online) The contribution of the proximity-induced magnetism on TI surface states. (a) Quantum correction prefactors as a function of temperature, where α_1 for the WAL term is marked in the blue region, while α_2 for the WL component is in the red region. (b) Temperature-dependent phase coherence length l_Φ for WAL in pure Bi_2Se_3 and heterostructure. Both curves follow the power law function $T^{-\beta}$ with $\beta \sim 0.42$. The error bars in (a) and (b) describe the deviation during the HLN fitting process. (c) The conductance variation as the temperature increases for pure Bi_2Se_3 and the heterostructure. The logarithmic increase corresponds to the quantum correction in the conductivities. (d) A sketch of the band structure in Bi_2Se_3 before and after integrating with Mn_xGe_{1-x}. By proximity effect, a bandgap could be opened in the Dirac cone of the bottom surface.

Supplementary File. Such logarithmic behavior results from the combined effect of quantum corrections induced by WAL, WL, and electron-electron interaction (EEI) effects [40]. In general, the quantum correction from WAL and WL can be described as [41]

$$\Delta\sigma_{xx}^{\mathrm{WAL(WL)}} = \frac{\alpha_i \beta_i e^2}{\pi^2 \hbar} \ln\left(\frac{T}{T_L}\right), \tag{3}$$

where T_L is the characteristic temperature when the quantum correction vanishes, α_i and β_i are the factors fitted from (2), $i = 1$ represents the WAL component, and $i = 2$ stands for the WL component. Following this equation, the contribution of quantum correction from WAL in pure Bi_2Se_3 ($\Delta\sigma_{xx}^{\mathrm{TI}}$) and the heterostructure ($\Delta\sigma_{xx}^{\mathrm{Bilayer}}$) can be calculated by adopting the extracted α_i and β_i values from Figures 4(a) and (b). Notably, owing to the leading role of WAL in Bi_2Se_3's transport channel, the conductance is expected to present a negative slope with the temperature increases because of the negative WAL prefactor. However, the pure Bi_2Se_3 shows a conductance increase in the quantum diffusive regime (blue line in Figure 4(c)). Previous reports have indicated the additional conductance increase comes from the EEI term $\Delta\sigma_{xx}^{\mathrm{EEI}}$ in Bi_2Se_3 thin film [41, 42], which will cause an increase in the surface conductance. Therefore, the overall conductance variation for pure Bi_2Se_3 in the quantum can be described as $\Delta\sigma_{xx}^{\mathrm{TI}} = \Delta\sigma_{xx}^{\mathrm{WAL}} + \Delta\sigma_{xx}^{\mathrm{EEI}}$. Here the value of $\Delta\sigma_{xx}^{\mathrm{TI}}$ can be estimated by (3) as $0.12e^2/h$, while $\Delta\sigma_{xx}^{\mathrm{WAL}}$ can be calculated using the parameter obtained in (1) as $\Delta\sigma_{xx}^{\mathrm{WAL}} = -0.07e^2/h$. Finally, the quantum correction of EEI can be calculated as $0.19e^2/h$. Along this line, in Bi_2Se_3/Mn_xGe_{1-x}, the contribution of WAL and WL can be calculated using the fitting parameter from (2) as $\Delta\sigma_{xx}^{\mathrm{WAL}} = -0.06e^2/h$ and $\Delta\sigma_{xx}^{\mathrm{WL}} = 0.26e^2/h$, while the overall quantum correction is $\Delta\sigma_{xx}^{\mathrm{Bilayer}} = \Delta\sigma_{xx}^{\mathrm{WL}} + \Delta\sigma_{xx}^{\mathrm{WAL}} + \Delta\sigma_{xx}^{\mathrm{EEI}} = 0.39e^2/h$. This value is very close to the experiment value in Figure 4(c) ($\Delta\sigma_{xx}^{\mathrm{Bilayer}} \sim 0.4e^2/h$), confirming the accuracy of our fitting results in the quantum interference picture, which are correlated to the proximity-induced magnetic order in the Bi_2Se_3 film. Figure 4(d) shows the band structures of pure Bi_2Se_3 and Bi_2Se_3/Mn_xGe_{1-x} heterostructures. Considering the relatively small proximity length [16], we propose that the bandgap is

opened in the Dirac cone of the bottom surface.

In addition, the bandgap induced in the surface state can be calculated with the obtained α_1 and α_2 in (3), since the prefactors of WAL and WL in Bi_2Se_3 are explicit functions of gap size Δ and Fermi level E_F [43]. After careful examination (as discussed in Appendix D in the Supplementary File), the E_F position of the Bi_2Se_3 layer is calculated to be 113 meV at 1.9 K, and the opening bandgap size is 80 meV. This value is at the same level with magnetically doped TIs (for example, the Cr doping can open a bandgap with a size of 70–90 meV in Bi_2Se_3 [44] or $(Bi_xSb_{1-x})_2Te_3$ [45]), which indicates that the proximity effect is an effective method to induce a bandgap in TI surface states. Previous reports indicated that a large bandgap can be opened in Bi_2Se_3/YIG ($\sim$70 meV) [33] and $MnBi_2Te_4/Bi_2Te_3/MnBi_2Te_4$ heterostructures (70 ± 15 meV) [46], proving the potential of proximity effect for realizing the TI-based quantum devices.

3 Conclusion

In summary, we demonstrate a Bi_2Se_3/Mn_xGe_{1-x} heterostructure prepared by MBE, and multiple characterization methods are used to verify the good crystal quality and morphology of our sample. By precisely controlling the sample stoichiometry, we separate the transport properties of the Bi_2Se_3 layer from the heterostructure and observe a reversed AHE curve, which proves that magnetism is induced by the interfacial proximity effect. Different from pure TI where the magnetoresistance curve exhibits a WAL feature, after integrating with Mn_xGe_{1-x}, the magnetoresistance in the Bi_2Se_3 layer presents a typical WL feature, proving that the proximity-induced magnetism can exist until 150 K. Detailed fitting about the magnetoconductance quantifies this transition from WAL to WL and suggests that a surface bandgap could be opened by the magnetism. Furthermore, we compared the theoretical and experimental quantum correction induced by WAL and WL, proving the accuracy of our fitting results in the quantum interference picture and confirming the bandgap opening in Bi_2Se_3's surface states. The bandgap size is calculated to be 80 meV by adopting the fitting parameter. Our observation is of great importance for further understanding the mechanism of proximity-induced magnetism in topological insulators and provides a new strategy to modulate the topological surface states at high temperatures without introducing pollution and impurity.

Acknowledgements This work was supported by National Natural Science Foundation of China (Grant Nos. 62274009, 61774013), National Key R & D Program of China (Grant No. 2018YFB0407602), and International Collaboration Project (Grant No. B16001).

Supporting information Appendixes A–D. The supporting information is available online at info.scichina.com and link.springer.com. The supporting materials are published as submitted, without typesetting or editing. The responsibility for scientific accuracy and content remains entirely with the authors.

References

1 Hao Y, Xiang S Y, Han G Q, et al. Recent progress of integrated circuits and optoelectronic chips. Sci China Inf Sci, 2021, 64: 201401
2 Wang L D, Cai W L, Cao K H, et al. Femtosecond laser-assisted switching in perpendicular magnetic tunnel junctions with double-interface free layer. Sci China Inf Sci, 2021, 65: 142403
3 Cai W L, Wang M X, Cao K H, et al. Stateful implication logic based on perpendicular magnetic tunnel junctions. Sci China Inf Sci, 2022, 65: 122406
4 Eimer S, Cheng H Y, Li J J, et al. Perpendicular magnetic anisotropy based spintronics devices in Pt/Costacks under different hard and flexible substrates. Sci China Inf Sci, 2023, 66: 122408
5 Zhang D, Shi M, Zhu T, et al. Topological axion states in the magnetic insulator $MnBi_2Te_4$ with the quantized magnetoelectric effect. Phys Rev Lett, 2019, 122: 206401
6 Zang J, Nagaosa N. Monopole current and unconventional Hall response on a topological insulator. Phys Rev B, 2010, 81: 245125
7 Chang C Z, Zhang J, Feng X, et al. Experimental observation of the quantum anomalous Hall effect in a magnetic topological insulator. Science, 2013, 340: 167–170
8 Kou X, Guo S T, Fan Y, et al. Scale-invariant quantum anomalous Hall effect in magnetic topological insulators beyond the two-dimensional limit. Phys Rev Lett, 2014, 113: 137201
9 Kou X, Fan Y, Lang M, et al. Magnetic topological insulators and quantum anomalous hall effect. Solid State Commun, 2015, 215-216: 34–53
10 Kou X, Lang M, Fan Y, et al. Interplay between different magnetisms in Cr-doped topological insulators. ACS Nano, 2013, 7: 9205–9212
11 Kou X F, Jiang W J, Lang M R, et al. Magnetically doped semiconducting topological insulators. J Appl Phys, 2012, 112: 063912
12 Zhang L, Zhao D, Zang Y, et al. Ferromagnetism in vanadium-doped Bi_2Se_3 topological insulator films. APL Mater, 2017, 5: 076106
13 Carva K, Baláž P, Šebesta J, et al. Magnetic properties of Mn-doped Bi_2Se_3 topological insulators: ab initio calculations. Phys Rev B, 2020, 101: 054428

14 Sánchez-Barriga J, Varykhalov A, Springholz G, et al. Nonmagnetic band gap at the Dirac point of the magnetic topological insulator $(Bi_{1-x}Mn_x)_2Se_3$. Nat Commun, 2016, 7: 10559
15 Checkelsky J G, Yoshimi R, Tsukazaki A, et al. Trajectory of the anomalous Hall effect towards the quantized state in a ferromagnetic topological insulator. Nat Phys, 2014, 10: 731–736
16 Katmis F, Lauter V, Nogueira F S, et al. A high-temperature ferromagnetic topological insulating phase by proximity coupling. Nature, 2016, 533: 513–516
17 Yao X, Gao B, Han M G, et al. Record high-proximity-induced anomalous hall effect in $(Bi_xSb_{1-x})_2Te_3$ thin film grown on $CrGeTe_3$ substrate. Nano Lett, 2019, 19: 4567–4573
18 Lang M, Montazeri M, Onbasli M C, et al. Proximity induced high-temperature magnetic order in topological insulator-ferrimagnetic insulator heterostructure. Nano Lett, 2014, 14: 3459–3465
19 Tang C, Chang C Z, Zhao G, et al. Above 400-K robust perpendicular ferromagnetic phase in a topological insulator. Sci Adv, 2017, 3: e1700307
20 He Q L, Kou X, Grutter A J, et al. Tailoring exchange couplings in magnetic topological-insulator/antiferromagnet heterostructures. Nat Mater, 2017, 16: 94–100
21 He Q L, Yin G, Grutter A J, et al. Exchange-biasing topological charges by antiferromagnetism. Nat Commun, 2018, 9: 2767
22 Liu W, Zhang H, Shi J, et al. A room-temperature magnetic semiconductor from a ferromagnetic metallic glass. Nat Commun, 2016, 7: 13497
23 Matsukura F, Tokura Y, Ohno H. Control of magnetism by electric fields. Nat Nanotech, 2015, 10: 209–220
24 Park Y D, Hanbicki A T, Erwin S C, et al. A group-IV ferromagnetic semiconductor: Mn_xGe_{1-x}. Science, 2002, 295: 651–654
25 Murata K, Kirkham C, Tsubomatsu S, et al. Atomic layer doping of Mn magnetic impurities from surface chains at a Ge/Si hetero-interface. Nanoscale, 2018, 10: 295–301
26 Kim S, Lee S, Woo J, et al. Growth of Bi_2Se_3 topological insulator thin film on Ge(1 1 1) substrate. Appl Surf Sci, 2018, 432: 152–155
27 He L, Xiu F, Wang Y, et al. Epitaxial growth of Bi_2Se_3 topological insulator thin films on Si (111). J Appl Phys, 2011, 109: 103702
28 He L, Xiu F, Yu X, et al. Surface-dominated conduction in a 6 nm thick Bi_2Se_3 thin film. Nano Lett, 2012, 12: 1486–1490
29 Zhang D, Richardella A, Rench D W, et al. Interplay between ferromagnetism, surface states, and quantum corrections in a magnetically doped topological insulator. Phys Rev B, 2012, 86: 205127
30 Liu N, Teng J, Li Y. Two-component anomalous Hall effect in a magnetically doped topological insulator. Nat Commun, 2018, 9: 1282
31 Liu W, West D, He L, et al. Atomic-scale magnetism of Cr-doped Bi_2Se_3 thin film topological insulators. ACS Nano, 2015, 9: 10237–10243
32 Gracia-Abad R, Sangiao S, Bigi C, et al. Omnipresence of weak antilocalization (WAL) in Bi_2Se_3 thin films: a review on its origin. Nanomaterials, 2021, 11: 1077
33 Che X, Murata K, Pan L, et al. Proximity-induced magnetic order in a transferred topological insulator thin film on a magnetic insulator. ACS Nano, 2018, 12: 5042–5050
34 Hikami S, Larkin A I, Nagaoka Y. Spin-orbit interaction and magnetoresistance in the two dimensional random system. Prog Theor Phys, 1980, 63: 707–710
35 He H T, Wang G, Zhang T, et al. Impurity effect on weak antilocalization in the topological insulator Bi_2Se_3. Phys Rev Lett, 2011, 106: 166805
36 Lang M, He L, Kou X, et al. Competing weak localization and weak antilocalization in ultrathin topological insulators. Nano Lett, 2013, 13: 48–53
37 Lu H Z, Shen S Q. Weak localization of bulk channels in topological insulator thin films. Phys Rev B, 2011, 84: 125138
38 Xu S Y, Neupane M, Liu C, et al. Hedgehog spin texture and Berry's phase tuning in a magnetic topological insulator. Nat Phys, 2012, 8: 616–622
39 Altshuler B L, Aronov A G, Khmelnitsky D E. Effects of electron-electron collisions with small energy transfers on quantum localisation. J Phys C-Solid State Phys, 1982, 15: 7367–7386
40 Bardarson J H, Moore J E. Quantum interference and Aharonov-Bohm oscillations in topological insulators. Rep Prog Phys, 2013, 76: 056501
41 Jing Y, Huang S, Zhang K, et al. Weak antilocalization and electron-electron interaction in coupled multiple-channel transport in a Bi_2Se_3 thin film. Nanoscale, 2016, 8: 1879–1885
42 Liu M, Chang C Z, Zhang Z, et al. Electron interaction-driven insulating ground state in Bi_2Se_3 topological insulators in the two-dimensional limit. Phys Rev B, 2011, 83: 165440
43 Lu H Z, Shi J, Shen S Q. Competition between weak localization and antilocalization in topological surface states. Phys Rev Lett, 2011, 107: 076801
44 Chang C Z, Tang P, Wang Y L, et al. Chemical-potential-dependent gap opening at the Dirac surface states of Bi_2Se_3 induced by aggregated substitutional Cr atoms. Phys Rev Lett, 2014, 112: 056801
45 Lee I, Kim C K, Lee J, et al. Imaging Dirac-mass disorder from magnetic dopant atoms in the ferromagnetic topological insulator $Cr_x(Bi_{0.1}Sb_{0.9})_{2-x}Te_3$. Proc Natl Acad Sci USA, 2015, 112: 1316–1321
46 Li Q, Trang C X, Wu W, et al. Large magnetic gap in a designer ferromagnet-topological insulator-ferromagnet heterostructure. Adv Mater, 2022, 34: 2107520